The Induction Hardening Response and Fatigue Properties of Ferrite and Pearlite Banded 4145 Steel

Patrick I. Anderson
The Timken Company
P.O. Box 6930
Mail Code: RES-13
Canton, OH 44706-0930
Tel: 330-471-2260
Fax: 330-471-2282
E-mail: patrick.anderson@timken.com

David K. Matlock and John G. Speer
Advanced Steel Processing and Products Research Center
Colorado School of Mines
Golden, CO 80401
Tel: 303-273-3025
Fax: 303-273-3016
E-mail: dmatlock@mines.edu and jspeer@mines.edu

Key words: Banding, Fatigue, Induction Hardening, Chemical Segregation, Anisotropic Properties

INTRODUCTION

Induction hardening provides an efficient and versatile method for surface and through-hardening of steel components. Numerous component designs take advantage of the increased strength and compressive residual stresses generated at the surface of case hardened parts to improve fatigue life. However, there is concern regarding the uniformity of properties in induction heat treated parts, specifically when hardening heterogeneous microstructures containing alternating composition bands. Effects of prior microstructure homogeneity must be understood to ensure an optimum induction hardened part.

Numerous studies have connected effects of chemical segregation to tensile and impact toughness properties[1-5]. However, availability of data relating microchemical and/or microstructural banding to fatigue behavior is limited. Recent work by Coryell shows that induction hardening response is dependent on prior microstructure[6]. With an increased number of parts being hardened by induction due to process efficiency and reduced cost, there is increased concern that all parts achieve the same result. Heavily banded microstructures could display non-uniform response to the rapid heating rates employed by induction hardening by creating hardened parts with property gradients. These parts could meet outward hardness criteria yet have different case microstructures that may exhibit inferior performance in service. A non-ideal case microstructure could increase susceptibility to fatigue failure. The purpose of this paper is to present the results of a novel experiment designed to systematically evaluate the fatigue properties of induction hardened banded materials as a function of band orientation, prior microstructure, and induction hardening parameter.

EXPERIMENTAL PROCEDURES

A novel experimental plan, designed to provide cylindrical rotating bending fatigue (RBF) samples with compositional banding of consistent wavelength with bands oriented either parallel or perpendicular to the sample axis, was employed in this study and a complete summary of experimental procedures is presented elsewhere[7]. To facilitate sample selection at a controlled radial position, a 171 mm diameter hot rolled bar was used, involving modified 4145 (4145M) steel with a Mn content of 1.04 wt pct. which is slightly higher than normal having the composition shown in Table I. Manganese is known to affect development of microstructural banding during steel processing, and carbon is in the range commonly used for induction hardened components[8]. Blanks were

prepared following the sequence illustrated in Figure 1. The bar center was removed by trepanning to form a tube with a 51 mm wall thickness. The tube was trisected longitudinally and each section was hot rolled flat to form plates of approximately 45 mm thickness. Flat 12.5 mm plates were removed from the flattened sections. Longitudinal (i.e. parallel to the original bar rolling direction) and transverse (i.e. perpendicular to the original bar rolling direction) samples were machined from the flat plates such that the gage sections of the fatigue samples were all located at the same radial position with respect to the original bar.

Table I Comparison of the 4145M alloy used in this investigation with nominal composition ranges for 4145 steel (in wt pct.)

Steel	C	Mn	P	S	Si	Cr	Ni	Mo	Cu	Al	N
4145M	0.46	1.04	0.008	0.012	0.21	1.15	0.13	0.33	0.22	0.032	0.0091
4145	0.43/0.48	0.75/1.00	0.030 max	0.040 max	0.15/0.35	0.80/1.10	0.25 max	0.15/0.25	---	---	---

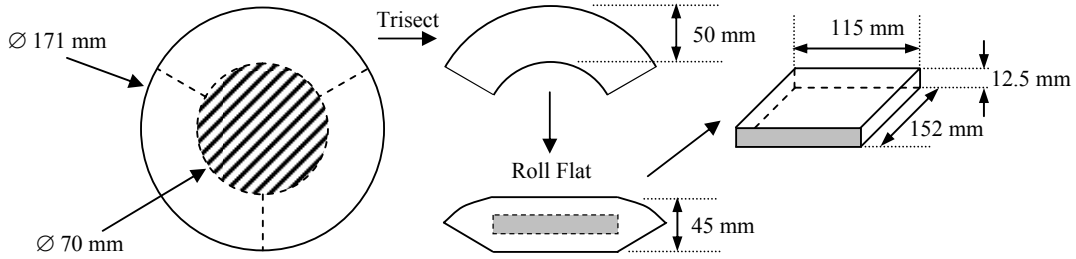

Figure 1 Schematic drawings of the fatigue sample blank removal method. The process includes trepanning the center of the round, trisecting the remaining tube, hot rolling these sections into flat plate, and removing the center material for machining into sample blanks. All dimensions in mm.

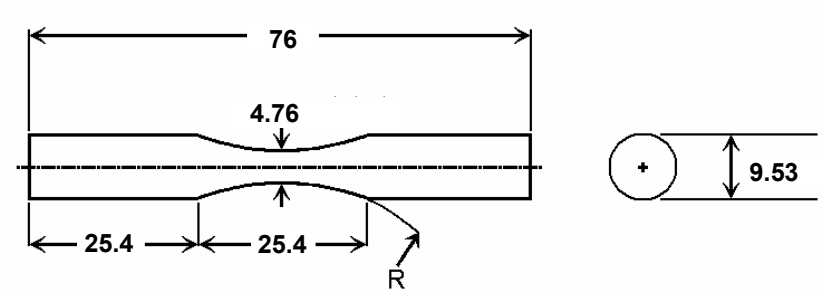

Figure 2 Schematic of the RBF test sample used in this research. All dimensions in mm.

The 4145M was heat treated to produce two different starting microstructures, both composed of ferrite and pearlite. One heat treatment (900 °C (1650 °F) for 30 minutes, furnace cool) produced the heterogeneous material, consisting of alternating bands of ferrite and pearlite, which is shown in Figure 3a. For the other heat treatment, material underwent a high temperature homogenization heat treatment (1200 °C (2200 °F) for 100 hours, 2 grain refinement HT cycles, furnace cool) to produce the equiaxed ferrite and pearlite microstructure shown in Figure 3b. The high temperature and duration were necessary for substitutional alloy diffusion given the material's average banding wavelength. The chemical segregation was modeled[7] using a sinusoidal function and the homogenization heat treatment was designed to reduce the Mn segregation amplitude to 5% of the original value. The hardnesses of the two starting microstructures were essentially the same, approximately 95 HRB, independent of orientation. In addition to creating an equiaxed microstructure, the homogenization treatment also changed the morphology of the MnS inclusions present in the as-received steel. The elongated MnS inclusions tended to disassociate along their length and then spheroidize, with their average aspect ratio decreasing from 7.4 to 2.5 and their average length decreasing from 15.3 μm to 7.6 μm upon homogenization.

The RBF samples were induction hardened along the entire gage section. Induction hardening parameters were varied to examine the differences in final case microstructure and fatigue properties that could be produced with slight changes to induction heat treatments, thus imitating possible variations in an industrial hardening environment. Through five sets of induction parameters, which are detailed in Table II, three variables were altered: induction duration, power input and quench dwell duration. These three variables

were chosen because of their ability to alter case depth and case/core transition zone characteristics. For variations A-C, duration was altered. For variations D-E, power input was lowered and duration kept the same as A. For variation E, a quench dwell was added. For all other variations the quench was applied immediately after the induction coil shut off, however, the quench dwell added a delay time between coil shut off and quench. All samples were single shot induction hardened, while rotating at 400 rpm, followed by a quench with 9 pct. polymer in water. All induction hardened test groups showed nearly identical straightness values to those of pre-induction hardened RBF samples, demonstrating that the microchemical segregation did not have an effect on distortion of the RBF samples. After induction hardening, all RBF samples were tempered for 1 hour at 150 °C (300 °F) and shipped, by ground, back to the fatigue testing facility.

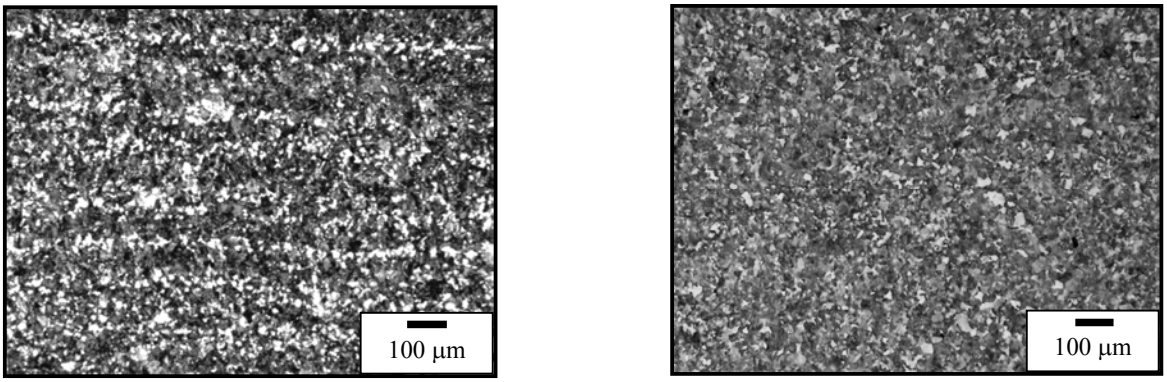

(a) (b)

Figure 3 Light optical micrographs of the microstructure created by the (a) ferrite and pearlite banding heat treatment and (b) homogenization heat treatment. Banding is parallel to rolling direction, which is the horizontal axis in both micrographs. 2 pct. nital etch.

Table II Induction Hardening Parameters Used to Process Fatigue Samples

Induction Designation	Power (kW)	Frequency (kHz)	Duration (s)	Quench Dwell (s)
A	189	312	0.32	---
B	189	312	0.31	---
C	189	312	0.33	---
D	182	312	0.32	---
E	182	312	0.32	0.25

The RBF tests were performed on four Model RBF-200 rotating beam fatigue testing machines. The machines were calibrated to ensure a statistically single population of data was produced. Prior to testing, all RBF samples were cleaned with ethanol in an ultrasonic bath to remove oil and other shipping residues. Applied fatigue stresses were selected to ensure RBF failures at the surface after at least 10^4 cycles. All samples were run until failure or runout at 10^7 fatigue cycles.

The material response to prior microstructure, banding orientation and induction hardening variation were shown through RBF performance and further defined with fractographic inspection, microstructural evaluation, banding characterization, inclusion analysis, Knoop microhardness profiles, and Woodvine stress analysis[7]. The different fatigue test groups were identified with three letters as follows: the first letter designates the orientation with respect to the rolling direction, either longitudinal (L) or transverse (T); the second letter designates the prior microstructure, either banded (B) or homogenized (H); and the third letter designates the applied induction hardening parameters, either A, B, C, D or E. Induction hardening parameters are each defined in Table II. At times, groups are referred to with only two letters in the following text. In these cases, the induction hardening parameters are not specified for the current discussion. In total there were 17 fatigue test groups: LB(A-E), TB(A-E), LH(A-C), and TH(A-D).

RESULTS

Induction Hardening Response

Microstructural homogeneity had a distinct influence on the response of a material to induction hardening. For RBF samples with the banded prior microstructure, which were sub-critically hardened, a heterogeneous banded microstructure was evident in all regions

(case, transition and core) of the final induction hardened part. Figure 4 shows an example of incomplete hardening near the surface of a transverse banded sample (TBA) where a ferrite band extends from the core to the surface. The microstructural banding also correlated to fluctuations in the hardness as demonstrated in Figure 5 which compares Knoop microhardness profiles for the transverse banded B (TBB) and transverse homogenized B (THB) samples. Predominant hardness fluctuations are evident in the banded material and are relatively absent in the homogenized sample. The hardness fluctuations associated with microstructural variations may be viewed as "metallurgical notches" in fatigue samples. Metallurgical notches were noted by Walker in improperly quenched parts[9]. Walker stated that localized surface areas that were not fully hardened could cause metallurgical notches where there is an incongruity in mechanical properties. Here, the concept is applied to non-uniform case depths, where small variations in microstructure cause variations in local mechanical properties on the scale of the original banding wavelength. When the metallurgical notches of lower yield strength material were stressed, preferential band deformation could have occurred, as documented by Fukuda *et al.*[10]. Fukuda *et al.* found that, in static torsion tests of banded steel, there was preferential deformation occurring in the ferrite bands rather than pearlite bands.

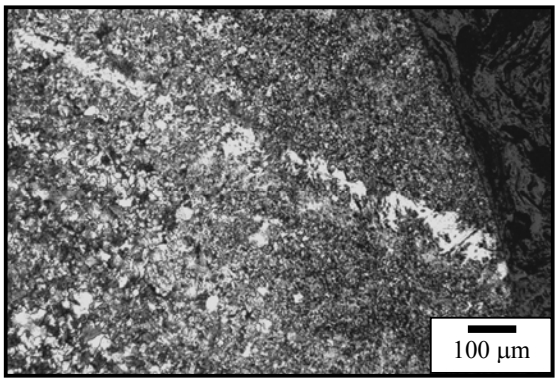

Figure 4 Light optical micrograph of post induction hardened 4145M microstructure showing a band of ferrite remaining from core to surface in a transverse banded sample (TBA) (2 pct. nital etch).

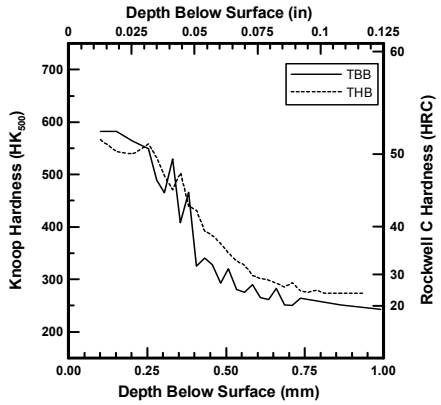

Figure 5 Knoop microhardness profiles for the transverse banded and transverse homogenized test groups with induction parameters B: 189 kW, 0.31 s, immediate quench. Plot extends only to a depth of 1 mm (0.125 in) to clarify the case and transition regions, which show that the THB material has a smoother curve with fewer, lower amplitude, hardness fluctuations.

The effect of induction parameter variation on test samples was measured using their respective case depth changes. Table III summarizes the primary hardness data used to characterize the heat treatments and Table IV summarizes average changes in depth to HRC 40 and total hardened depth (here being defined as the depth where the core hardness plateau is reached). The surface hardness depended slightly on orientation with the longitudinal samples exhibiting slightly higher surface hardness values, and the hardened depths differed significantly between induction hardening parameters. The power input had the largest effect on case depth to HRC 40, +0.13 mm, while the addition of a quench dwell significantly increased the total hardened depth, on average +0.18 mm, or 7.6% of the gage radius. The second increase in duration (from 0.32 s to 0.33 s) affected both depth to HRC 40, +0.12 mm (5% of

gage radius), and total hardened depth, +0.22 mm (9.2% of gage radius). To put these average increase values in perspective of the actual depths achieved in the samples, the average depth to HRC 40 was 20% of gage radius, while average total hardened depth was 35%.

Table III Summary of Experimental Test Matrix and Post-Induction Microhardness Data

Material Group Label	Surface Hardness (HRC)	Depth to 40 HRC (mm)	Total Hardened Depth (mm)
LBA	55	0.57	0.76
LBB	55	0.51	0.66
LBC	57	0.70	1.02
LBD	55	0.52	0.76
LBE	58	0.64	0.95
LHA	55	0.50	0.96
LHB	56	0.48	0.97
LHC	56	0.64	1.35
TBA	49	0.48	0.76
TBB	52	0.39	0.69
TBC	55	0.59	0.84
TBD	47	0.19	0.53
TBE	43	0.11	0.69
THA	46	0.48	0.71
THB	51	0.42	0.74
THC	54	0.57	0.86
THD	55	0.42	0.71

Table IV Summary of Case Depth Changes Due to Induction Parameter Variation

Induction Parameter	Initial Value	Increased Value	Average Change in Depth to HRC 40 (mm)	Average Change in Total Hardened Depth (mm)
Duration	0.31 s	0.32 s	+ 0.06	+ 0.01
	0.32 s	0.33 s	+ 0.12	+ 0.22
Power Input	182 kW	189 kW	+ 0.13	+ 0.08
Quench Dwell	0 s	0.25 s	+ 0.02	+ 0.18

Fatigue Behavior

Figure 6 compares fatigue data, plotted as stress versus number of cycles to failure, showing longitudinal and transverse orientations for both banded (Figure 6a) and homogenized (Figure 6b) starting microstructures. Due to the number of variables and available samples, stress amplitudes were chosen to produce failures at stress levels slightly greater than apparent endurance limits. As shown in Figure 6a, for the banded material the longitudinal SN curves exhibited a lower sensitivity to stress (i.e. lower slope) and higher stress values at all fatigue lives, i.e. 100-175 MPa (14-25 ksi) greater than the transverse curves of similar induction parameters. Results for induction variations B – E were similar to this LB and TB comparison. Correspondingly, as shown in Figure 6b for the homogenized material, the longitudinal SN curves are 25-125 MPa (4-18 ksi) greater than the transverse curves of similar induction parameters. The homogenized orientation comparisons for induction parameters A and B overlap statistically for higher stress levels yet were different for lower stress levels.

Figure 7 compares the effects of prior microstructure (i.e. banded versus homogenized) on RBF properties. For longitudinal samples, the fatigue properties of a given induction hardening parameter were independent of prior microstructure as illustrated in Figure 7a for induction processing parameter A. Similar results were also shown for induction processing parameters B and C[7]. In contrast, for all induction processing conditions, for transverse samples the fatigue behavior of the homogenized material was higher than the banded material by approximately 50-100 MPa (7-14 ksi). This difference is illustrated in Figure 7b for induction processing parameter C.

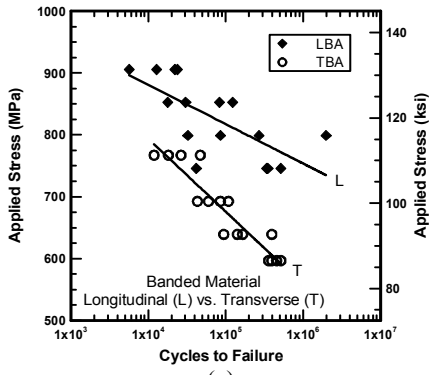

(a)

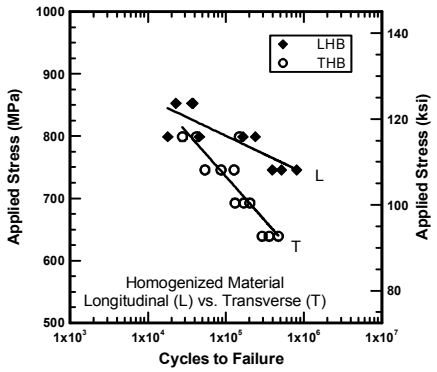

(b)

Figure 6 Stress versus cycles to failure plots for induction hardened 4145M under rotating bending fatigue showing anisotropic orientation effect on fatigue data. The longitudinal and transverse comparison for (a) banded material shows a 100-175 MPa (14-25 ksi) increase for longitudinal while (b) homogenized material shows a 25-125 MPa (4-18 ksi) increase for the longitudinal orientation.

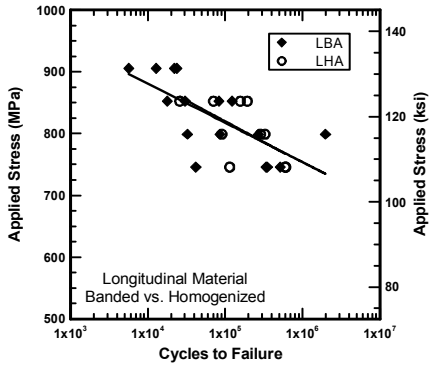

(a)

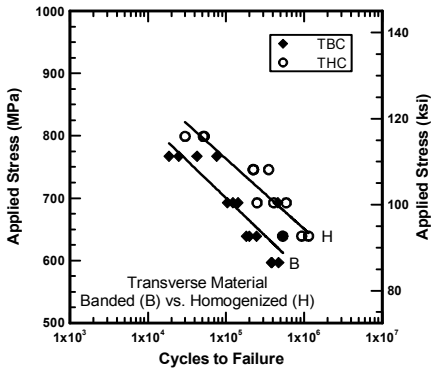

(b)

Figure 7 Stress versus cycles to failure plots for induction hardened 4145M under rotating bending fatigue showing effects of prior microstructure on fatigue data. The banded and homogenized comparison for (a) longitudinal material shows no difference while the (b) transverse material shows a 50 MPa (7 ksi) increase after homogenization.

The effects of variations in induction hardening parameters on fatigue performance were considered through selected comparisons. It was anticipated that the increase in case depth, and corresponding increase in composite strength, associated with an increase in heating duration (0.31, 0.32 and 0.33 s for parameters B, A and C, respectively) would lead to an increase in fatigue life as long as the residual stress profile was not significantly altered. Thus it was predicted that condition C would have the best fatigue performance, followed by condition A and then condition B. This B-A-C progression of improving fatigue response was found in three of the four orientation/prior microstructure combinations (longitudinal banded (LB), transverse banded (TB) and transverse homogenized (TH)). The longitudinal homogenized (LH) material exhibited sufficient scatter that the A and C curves overlapped, with the B curve being below them. This trend is shown, for the TB material, in Figure 8a. For the LB and LH materials all three SN curves were statistically similar, but for TB and TH the curves showed differentiation between the B and C induction parameters. These induction parameters were the two extremes of duration investigated.

The second induction comparison, A vs. D, was based on a change in power input. The power input values for A and D were 189 kW and 182 kW, respectively. It was hypothesized that an increase in power input would provide better fatigue response due to the increased heat input, and thus increase the case depth. Of the three orientation-microstructure groups where this comparison applied (TH, TB, LB), one followed the D-A progression of improving fatigue response (TH), as illustrated by the data shown in Figure 8b, while two (TB, LB) followed the trend but had differing slopes that brought the data close to identical at some applied stress levels. All comparisons for induction parameters A and D were statistically similar[7].

The third induction comparison, D vs. E, was based on the addition of a quench dwell time. Parameter D involved quenching immediately after the induction coil shut off while E had a 0.25 s delay between the shut off of the induction coil and the quench. The goal of adding a quench dwell was to alter the transition zone between hardened case and core materials. Only the two banded

material groups provided this comparison and the results were inconclusive. In comparing induction parameters E and D for TB and LB material the partial SN curves overlapped halfway and were statistically similar. The TB and LB curves showed opposite overlaps as well, further confusing the effect of a quench dwell on fatigue behavior[7].

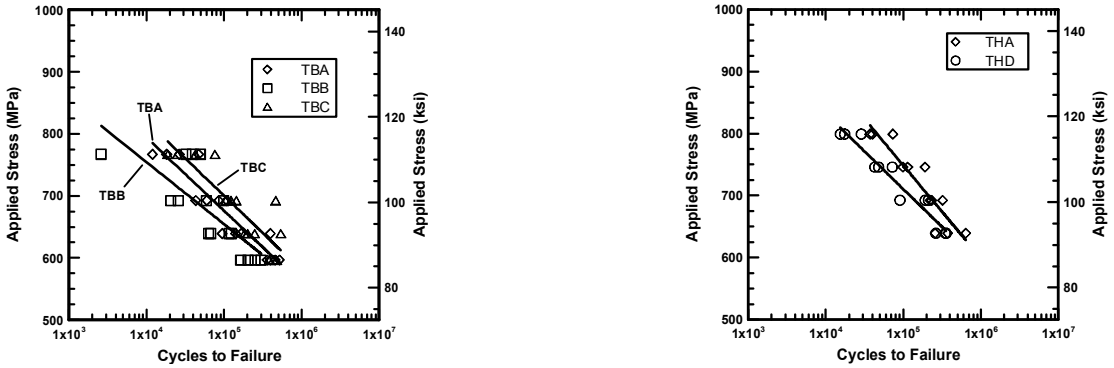

Figure 8 Stress versus cycles to failure for induction hardened 4145M under rotating bending fatigue showing effects of induction hardening parameters on fatigue data. (a) A comparison of the A, B and C induction hardening parameters (varying induction duration) for the TB material showing the expected B-A-C progression of improved fatigue properties. (b) A comparison of the A and D induction hardening parameters (varying induction power input) for the TH material showing the expected D-A progression of improved fatigue properties.

Failure initiation locations (surface or case/core interface) and types (inclusion or non-inclusion) were identified based on results of standard fractographic analysis techniques[7]. Overall, 71% of the all failures nucleated at inclusions, including 97% of transverse failures and 43% of longitudinal failures. The longitudinal inclusion failure percentage was probably higher, but root cause of initiation was difficult to detect on longitudinal fracture surfaces due to wear between mating fracture faces during testing. Of the 52% of failures that initiated at the case/core interface, all nucleated at MnS inclusions. The fact that inclusions caused a majority of fatigue failures implied that cleanliness of steel was vital to fatigue performance. These inclusions can also affect fatigue data scatter by producing failures when they would not occur in the absence of inclusions.

DISCUSSION

There are two main contributing factors to the induction response and fatigue behavior presented from this research: microstructural banding and MnS inclusions. The microstructural banding affected the induction hardening response by producing non-uniform hardness profiles in the banded 4145M. This led to incongruities in strength, and thus fatigue resistance, at the surface and at the case/core interface. The MnS inclusions were present in two different morphologies, depending on prior microstructure heat treatments. These two morphologies, elongated and spheroidized, interacted with the original banding orientation to produce both relatively beneficial and detrimental fatigue and fracture results.

The fatigue performance varied for each of the four main material groups, with longitudinal banded showing the longest fatigue life, followed by, in decreasing order, longitudinal homogenized, transverse homogenized and transverse banded. In addition to displaying unique fatigue response, each of the four test groups showed unique fracture characteristics. Standard fractographic investigation led to the discovery of many fracture differences between test groups[7]. A notable difference is the effect of MnS inclusions on fracture surface morphology. Upon homogenization, MnS evolved from an elongated to a spheroidized morphology as shown in Figures 9a and 9b. The corresponding fracture overload regions are shown in Figures 9c and 9d, respectively. In both cases the ductile void geometry mirrored the MnS morphology. The transverse banded voids in Figure 9c match the elongated nature of the inclusions, while the transverse homogenized voids in Figure 9d show a 'bamboo' like organization of small, linearly aligned voids. Figure 9 refers solely to the transverse test groups, however, the MnS inclusions affected fracture in the longitudinal orientation as well by causing cracks normal to the plane of maximum tension (parallel to sample axis) in the banded material. These cracks extended from the main fracture surface down to elongated inclusions in the steel matrix, effectively diverting the crack path and inhibiting crack propagation across the test sample.

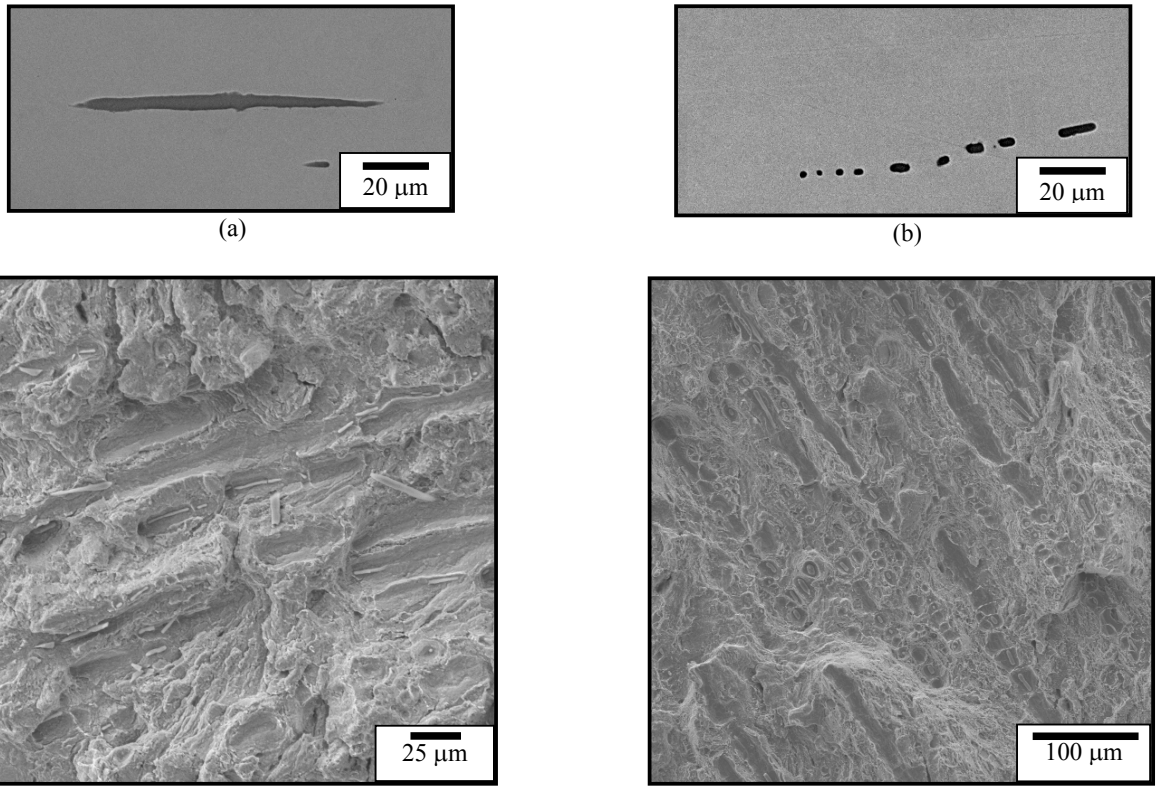

Figure 9 A collection of figures showing the effect of MnS shape on fracture surface morphology created during rotating bending fatigue. (a) and (b) show backscatter electron scanning electron microscope images of MnS inclusions showing the typical (a) as-received and (b) post-homogenized MnS shape. (c) and (d) show corresponding overload region fracture surfaces of (c) transverse banded and (d) transverse homogenized material. Both overload regions show ductile voids which mirror the respective MnS inclusion geometries shown in (a) and (b).

The synergistic effects of microstructural bands and MnS inclusions are just as important a factor to consider as their individual contributions. A challenge found when comparing banded and homogenized test samples from the same parent material is separating the influences of microstructural banding and MnS inclusion effects[2,5]. A consequence of long term, high temperature homogenization is the change in morphology of the MnS inclusions that causes an inclusion distribution different from the parent material. In this study, the percentage shift in fatigue behavior attributed individually to either inclusion effects or ferrite and pearlite microstructural banding effects was not quantified. However, in previous research, Grange stated that both influences are deleterious to mechanical properties and even accentuated by the presence of each other[2]. Both Grange and Spitzig assigned the primary responsibility for ductility, tensile and toughness property anisotropy in banded steels to MnS inclusions[2, 5]. In this study the major effect of microstructural banding was creating microstructural, and thus hardness and strength, gradients in the transition region of the induction hardened samples. These localized non-uniformities, i.e. metallurgical notches, played a role in the initiation of case/core interface cracks due to non-uniform work hardening of the soft core microstructure. The interaction of the work hardening in these metallurgical notches with local MnS inclusions could be a form of accentuation that supports the Grange hypothesis.

The longitudinal banded material showed the superior fatigue response of the four major test groups. This response is attributed to advantageous orientation of ferrite and pearlite structural banding and MnS inclusions to the fracture plane. In these samples ferrite and pearlite bands and MnS inclusions were elongated parallel to the banding. Ferrite and pearlite bands and elongated MnS inclusions provided increased resistance to nucleation and propagation of cracks. Manganese sulfide inclusions also acted as barriers to cracks, forcing cracks to fracture inclusions or travel around inclusion/matrix interfaces. The longitudinal homogenized test group provided the second best fatigue response. The difference in fatigue performance appeared slightly less, yet was statistically similar to the longitudinal banded material (all curves overlapped within plus/minus one standard deviation).

The transverse homogenized samples showed the third best fatigue performance. Transverse material as a whole was inferior to longitudinal material due to the increased availability of preferential crack paths along microstructural bands and elongated MnS inclusions, which initiated 97% of transverse fatigue cracks, thus shortening fatigue life. However, in this material the effects of

homogenization improved fatigue performance over transverse banded material, which had the lowest fatigue performance of the four material groups. This increase was because the preferential crack paths were reduced, in the transverse direction, by the homogenization heat treatment. Less continuous inclusion/matrix interface area was available in the fracture plane after homogenization, when the MnS inclusions spheroidized and became shorter. The lower fatigue response of the transverse banded material was due to the availability of preferential crack paths. Ferrite and pearlite bands and elongated MnS inclusions provided low energy crack paths through the transverse banded material. The transverse banded material also showed non-uniform response to induction hardening where metallurgical notches were created around the circumference of the case/core interface. Tensile testing showed that the yield strength of the core banded material was 414 MPa (60 ksi), which was below the calculated applied stress values near the transition zone in a majority of the test samples. During RBF, the lower strength regions in the transition zone notches yielded and work hardened during further cyclic stressing. It is assumed from literature that failures at inclusions can occur when there is a build up of localized strain without sufficient dislocations to dissipate the generated strain gradient[10]. In this case inclusion particles must deform, fracture, or disassociate from the matrix. It follows that a certain number of fatigue cycles would be required to create the critical strain field surrounding an inclusion necessary to cause one of the aforementioned inclusion responses. An inclusion located near or at the localized work-hardened region could have initiated a case/core failure prematurely, and/or unexpectedly, with ease, contributing to the inferior fatigue performance of the transverse banded material.

When measuring the case depth created by induction hardening, it is important to obtain an accurate value. Heterogeneous case microstructures produced by induction hardening, especially in the transverse banded material, could alter the ability to obtain accurate measurements and thus lead to over- or underestimation of fatigue properties. Evolution of case microstructure along bands into the core region could yield over-estimated case depth measurements if hardness traverses were taken along a former pearlite band. For ferrite and pearlite banded prior microstructures, the case depth would be limited to the depth to which the ferrite bands were hardened, also defined as the depth at which sufficient carbon diffusion in the austenite was allowed. In limiting the effective case depth, the unhardened ferrite bands also limit fatigue performance, as the samples with deeper case depths showed greater fatigue lives in this study.

CONCLUSIONS

1. Small changes in the induction hardening processing parameters showed a distinct influence on the final heat treated part. The duration, power input and quench dwell variations included in the test matrix produced large percentage differences in case depth indicators (Depth to HRC 40 and Total Hardened Depth).

2. Banded material showed preferential case hardening along carbon rich bands (pearlite). This response caused non-uniform case depths around the entire circumference of transverse banded material samples. This non-uniformity could lead to unexpected failure due to the formation of metallurgical notches and their interaction with surrounding MnS inclusions.

3. Banded material also showed fluctuations in hardness profiles. These fluctuations in hardness, and thus effective fatigue strength, were caused by heterogeneous banded regions in the prior microstructure and matched the dimensions of the pre-induction banding wavelength. These uneven hardness gradients showed that prior microstructure had a measurable effect in post-induction hardened parts. Homogenizing the microstructure prior to induction hardening reduced the frequency and amplitude of these hardness fluctuations.

4. Fatigue performance varied for each of the four main material groups; longitudinal banded showed the longest fatigue life, followed by, in decreasing order, longitudinal homogenized, transverse homogenized and transverse banded.

5. Elongated manganese sulfide inclusions strongly influenced the fatigue crack initiation of the RBF samples. Ninety-seven percent of transverse sample failures initiated at inclusions, either at the surface (35%) or the case/core interface (62%). Forty-three percent of longitudinal sample failures initiated at inclusions, all at the case/core interface. These inclusion initiated failures implied that material cleanliness was a key factor in fatigue performance.

6. Components produced from heterogeneous banded material parallel and perpendicular to banding did not have the same fatigue properties. The transverse banded and transverse homogenized materials produced partial SN curves 100-175 MPa and 25-125 MPa lower than their respective longitudinal counterparts. This difference was due to the preferential crack paths available in the transverse direction that eased fatigue crack nucleation and propagation. Homogenization of the prior microstructure was beneficial to fatigue properties only in the transverse oriented fatigue samples, where the predicted fracture plane was parallel to the banding plane (rolling direction). The fatigue properties were statistically similar for the longitudinal banded and longitudinal homogenized materials.

ACKNOWLEDGEMENTS

We would like to acknowledge the Advanced Steel Processing and Products Research Center, an industry/university cooperative research center, at the Colorado School of Mines for supporting this research. We would also like to acknowledge The Timken Company, Contour Hardening, Inc. and Los Alamos National Labs for providing research material and services during the course of this project.

REFERENCES

1. H. Schwartzbart, "Effect of Manganese Banding on Mechanical Properties of Heat Treated Steel Plate in the Thickness Direction," *Transactions of the ASM*, 1952, Vol. 44, pp. 845-852.

2. R.A. Grange, "Effect of Microstructural Banding in Steel," *Metallurgical Transactions*, 1971, Vol. 2, pp. 417-426.

3. C.F. Jatczak, D.J. Girardi, E.S. Rowland, "On Banding in Steel," *Transactions of the ASM*, 1956, Vol. 48, pp. 279-305.

4. M.A. Urzendowski, F.J. Worzala, "An Investigative Analysis of the Properties of Severely Segregated A441 Bridge Steel," *Conference: Analyzing Failures: the Problems and the Solutions*, Salt Lake City, UT, 2-6 Dec. 1985, ASM International, 1986, pp. 27-36.

5. W.A. Spitzig, "Effect of Sulfide Morphology and Pearlite Banding on Anisotropy of Mechanical Properties in Normalized C-Mn Steels," *Metallurgical Transactions A*, 1983, Vol. 14A, pp. 271-283.

6. J.J. Coryell, "The Effect Of Induction Hardening On The Mechanical Properties Of Steel With Controlled Prior Microstructures," M.S. Thesis, Colorado School of Mines, Golden, CO, August 2004.

7. P.I. Anderson, "Induction Hardening Response of Ferrite and Pearlite Banded Steel," M.S. Thesis, Colorado School of Mines, Golden, CO, December 2005.

8. W.C. Leslie, *The Physical Metallurgy of Steels*, Hemisphere Publishing Corporation, New York, NY, 1981, pp. 172-173.

9. E.D. Walker, " Some Aspects of Residual Stress in Parts Heat Treated by the Induction Method," *Conference: Residual Stress for Designers and Metallurgists*; Chicago, IL, 9-10 April 1980, ASM International, Materials Park, OH, 1981, pp. 41-50.

10. T. Fukuda, K. Fujimura, H. Nisitani, "Effects of Rolled Structure on the Fatigue of Carbon Steel Plain Specimens under Combined Stresses," *ICM8: Eighth International Conference on the Mechanical Behaviour of Materials*; Victoria, British Columbia; Canada; 16-21 May 1999, University of Alberta Department of Mechanical Engineering, Edmonton, Canada, 1999, pp. 201-204.

11. M.F. Ashby, "The Deformation of Plastically Non-Homogeneous Alloys," *Strengthening Methods In Crystals*, by A. Kelly and R. B. Nicholson, John Wiley & Sons, New York, NY, 1971, pp. 137-191.